LMM Auger primary excitation spectra of copper

Tougaard, Sven Mosbæk

Published in:
Surface Science

Publication date:
2014

Document version
Submitted manuscript

Citation for pulished version (APA):
Tougaard, S. M. (2014). LMM Auger primary excitation spectra of copper. Surface Science, 630, 294-299.

Surface Science 630 (2014) 294–299

Contents lists available at ScienceDirect

Surface Science

journal homepage: www.elsevier.com/locate/susc

LMM Auger primary excitation spectra of copper

N. Pauly [a,*], S. Tougaard [b], F. Yubero [c]

[a] Université Libre de Bruxelles, Service de Métrologie Nucléaire (CP 165/84), av. F. D. Roosevelt 50, B-1050 Brussels, Belgium
[b] Department of Physics, Chemistry and Pharmacy, University of Southern Denmark, DK-5230 Odense M, Denmark
[c] Instituto de Ciencia de Materiales de Sevilla (CSIC — Univ. Sevilla), av. Américo Vespucio 49, E-41092 Sevilla, Spain

ARTICLE INFO

Article history:
Received 24 July 2014
Received in revised form 29 August 2014
Accepted 31 August 2014
Available online 6 September 2014

Keywords:
Auger
LMM
Core-hole effect
Surface effect
Copper

ABSTRACT

The shape and intensity of measured Auger peaks are strongly affected by extrinsic excitations due to electron transport out of the surface and to intrinsic excitations induced by the sudden creation of the two static core holes. Following a method developed for XPS in a previous work [N. Pauly, S. Tougaard, F. Yubero, Surf. Sci. 620 (2014) 17], we have calculated the effective energy-differential inelastic electron scattering cross-sections, including the effects of the surface and of the two core holes, within the dielectric response theory by means of the QUEELS-XPS software (QUantitative analysis of Electron Energy Losses at Surfaces for XPS). The Auger spectra are then modeled by convoluting this energy loss cross section with the primary excitation spectrum that accounts for all effects which are part of the initial Auger process, i.e. L–S coupling and vacancy satellite effects. The shape of this primary excitation spectrum is fitted to get close agreement between the theoretical and the experimental spectra obtained from X-ray excited Auger electron spectroscopy (XAES). We have performed these calculations of XAES spectra for various LMM Auger transitions of pure Cu ($L_3M_{45}M_{45}$, $L_3M_{23}M_{45}$, $L_3M_{23}M_{23}$ and $L_2M_{45}M_{45}$ transitions). We compare the resulting primary excitation spectra with theoretical results published in the literature and obtain reasonable quantitative agreement. In particular, we extract from experimental spectra quantitative intensities due to Coster–Kronig, shake-off and shake-up processes relative to the intensity from the "normal" Auger process.

1. Introduction

Auger electron spectroscopy (AES) is currently a widely used characterization technique for probing the chemical and compositional properties of solid surfaces [1]. To perform practical quantitative AES, it is necessary to know specific parameters as ionization cross sections, electron back-scattering factors and Auger transition probabilities.

As for Auger transition probabilities, calculations have been available for a long time [2–4] but good agreement with experimental data was up to now never achieved. Note that the identification and quantification of Auger transitions is in general a very involved task because, in practice, the "normal" Auger emission after a photoemission process often overlaps with other competing Auger processes as for example the Auger decay in the presence of a spectator vacancy after a Coster–Kronig transition or other Auger processes where shake-up or shake-off states participate in the process [4,5].

Even recently, experimental determinations of Auger transition probabilities from X-ray excited Auger Electron Spectroscopy (XAES) were performed [6,7] but possibly their accuracy is poor due to the procedure, namely Shirley's method [8], used to carry out the background subtraction, i.e. the removal of intensity corresponding to energy losses due to inelastic scattering events experienced by the electrons after their initial excitation.

Indeed, it was previously shown [9] that background subtraction methods not only from Shirley [8] but also from Tougaard [10] (which intends to only correct for extrinsic excitations) do not take into account intrinsic losses, namely excitations due to the sudden creation of the static core-hole and the associated electric field, but only extrinsic excitations that take place during the photoelectron transport process which are due to the time and space varying electric field from the moving photoelectron. This fact blurs attempts to rigorously compare theoretical and XAES experimental results for Auger transition probabilities.

Recently a method was proposed [11,12] to determine the primary excited spectrum $F(E)$ (which accounts for all contributions that are part of the initial photoexcitation process) from a measured experimental XPS spectrum as well as the full simulated XPS spectrum. This method is based on a convolution of the energy-differential inelastic electron scattering cross-section for XPS, K_{sc}^{XPS}, including both extrinsic and intrinsic excitations, with the primary excitation spectrum, $F(E)$, which is considered as an input in the calculations. The energy loss cross section, K_{sc}^{XPS}, was determined with the QUEELS-XPS software (QUantitative

* Corresponding author at: Université Libre de Bruxelles, Service de Métrologie Nucléaire (CP 165/84), 50 av. F. D. Roosevelt, B-1050 Brussels, Belgium. Tel.: +32 2 6502083; fax: +32 2 6504534.
E-mail address: nipauly@ulb.ac.be (N. Pauly).

http://dx.doi.org/10.1016/j.susc.2014.08.029
0039-6028/

analysis of Electron Energy Losses at Surfaces for XPS) [13,14] which is based on the semiclassical dielectric response model [15,16].

In the present work, we show that the QUEELS-XPS software can also be used to calculate the energy-differential inelastic electron scattering cross-section, K_{sc}^{Auger}, valid to describe the electron transport related to an Auger emission process by assuming two static core-holes instead of one. Then, using the same procedure as in Refs. [11] and [12], we have modeled several XAES spectra of copper (more specifically the $L_3M_{45}M_{45}$, $L_3M_{23}M_{45}$, $L_3M_{23}M_{23}$ and $L_2M_{45}M_{45}$ transitions) and consequently obtain the full $F(E)$ primary excited spectra including all the terms contributing to each Auger cascade (terms resulting from L–S coupling of 2 or 3 holes) following the photoexcitation process. This analysis allows to quantify the relative Auger transition probabilities of the individual L–S coupling terms and also the relative importance of the relaxation processes contributing to the measured Auger spectra. The obtained results are compared with theoretical calculations published in Refs. [3] and [4].

In the next section we describe the model used in the QUEELS-XPS software as well as the procedure followed to obtain the primary excitation spectra $F(E)$ of the Auger transitions. The resulting contributions to $F(E)$ will then be compared to theoretical calculations for each individual Auger cascade.

2. Theoretical model

2.1. QUEELS formalism

The model implemented in QUEELS-XPS [13–15] is based on the surface reflection model [17] which describes the interactions of electrons with semi-infinite media in terms of the dielectric properties of the bulk material and incorporates the effects of the surface (when the electron travels both in the solid and in the vacuum), of the static core-hole(s) created during the photoionization process, as well as interference between these effects. The QUEELS-XPS formalism has been abundantly described in Ref. [15] and numerous examples of its validity have been reported in the literature [11,16,18,19] when one core-hole is considered, i.e. for XPS applications. To our knowledge, only one study [20] has been carried out for two core-holes, i.e. for Auger spectra with this model, and again a good agreement between theory and experiment was found. We only describe here the basic elements of the model.

We study here the case of an Auger cascade following the photoexcitation process and thus we consider an electron–hole-hole triplet created at a depth x_0 below the surface of a semi-infinite medium characterized by its dielectric function $\epsilon(\mathbf{k}, \omega)$. The electron travels along a straight line with velocity v, energy E and angle θ with respect to the surface normal, while the core holes are stationary with infinite lifetime. Within this model, the effective inelastic electron scattering cross section $K_{eff}^{AES}(E, \hbar\omega, x_0, \theta)$ is defined as the average probability that the electron, excited at depth x_0, loses an energy $\hbar\omega$ per unit energy loss and per unit path length traveled inside the solid (the *AES* in the expression of K_{eff} distinguishes this from the similar expression K_{sc}^{REELS} valid for a REELS experiment where the static core-hole is absent [21] and K_{sc}^{XPS} for XPS calculations with one core-hole).

The effective cross section, $K_{eff}^{AES}(E, \hbar\omega, x_0, \theta)$, is calculated for a single electron trajectory and it therefore depends on the depth x_0 where it is excited, but in XAES experiments electrons that contribute to the measured spectrum originate from a wide range of depths. Thus for comparison to experiments, it is necessary to perform a weighted average of $K_{eff}^{AES}(E, \hbar\omega, x_0, \theta)$ over all path lengths x traveled by the electrons which contribute to the spectrum with a weight function defined as the path-length distribution function for those electrons that have only undergone a single inelastic collision [15]. This results in the inelastic scattering cross-section $K_{sc}^{AES}(E, \hbar\omega, \theta)$ including bulk, surface and core hole effects as well as interferences between these effects.

We emphasize that the only input in the model to determine $K_{eff}^{AES}(E, \hbar\omega, x_0, \theta)$ and thus $K_{sc}^{AES}(E, \hbar\omega, \theta)$ is the dielectric function of the medium $\epsilon(\mathbf{k}, \omega)$ or, more precisely, the energy loss function (ELF) Im $\{-1/\epsilon(\mathbf{k}, \omega)\}$. To evaluate this latter, we consider as a model the expansion in Drude–Lindhard type oscillators [22]

$$\mathrm{Im}\left\{-\frac{1}{\epsilon(\mathbf{k},\omega)}\right\} = \sum_{i=1}^{n} \frac{A_i \hbar\gamma_i \hbar\omega}{\left(\hbar^2\omega_{0ik}^2 - \hbar^2\omega^2\right)^2 + \hbar^2\gamma_i^2\hbar^2\omega^2}\theta(\hbar\omega - E_G) \quad (1)$$

with the dispersion relation:

$$\hbar\omega_{0ik} = \hbar\omega_{0i} + \alpha_i \frac{\hbar^2 k^2}{2m}. \quad (2)$$

A_i, $\hbar\gamma_i$, $\hbar\omega_{0ik}$ and α_i are the strength, width, energy and dispersion of the ith oscillator, respectively and the step function $\theta(\hbar\omega - E_G)$ is included to describe the effect of the energy band gap E_G present in semiconductors and insulators. For the material studied in this work, namely copper, the parameters in the expansion are taken from Ref. [23].

Fig. 1 shows the resulting inelastic scattering cross-section K_{sc}^{AES} for electrons of 920 eV energy emitted from a copper sample at an angle $\theta = 15°$ with respect to the surface normal. This example has been chosen because it corresponds to one of the cases studied in this paper (Cu $L_3M_{45}M_{45}$ Auger electrons). Also shown in Fig. 1 are the inelastic scattering cross sections K_{sc}^{XPS}, K_{sc}^{REELS} and K_{inf} calculated for an electron of 920 eV energy traveling in the presence of one core-hole, in a REELS geometry (with 15° incidence and exit angles with respect to the surface normal) and in an infinite medium, respectively. We note that, for energy losses >30 eV the four spectra are similar, but for smaller energy losses, they deviate strongly. Thus, in comparison with K_{inf}, K_{sc}^{REELS} shows the effect of surface excitations, K_{sc}^{XPS} shows the additional effect of one static core-hole and finally K_{sc}^{AES} shows that two static core-holes further enhance the probability for energy loss.

2.2. Modeling XAES spectra

An XAES spectrum (as well as an XPS spectrum) can be seen as the addition of the contribution from electrons that have undergone an increasing number of energy loss events [24] and can be written

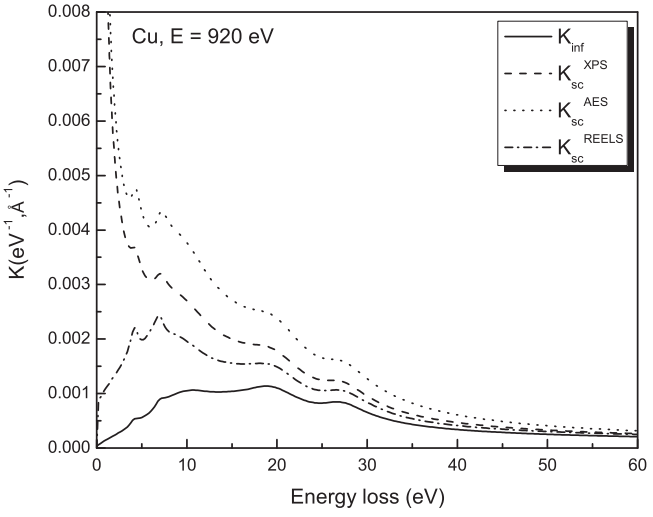

Fig. 1. $K_{inf}(E = 920\ eV, \hbar\omega)$ (solid line), $K_{sc}^{XPS}(E = 920\ eV, \hbar\omega, 15°)$ (dashed line), $K_{sc}^{AES}(E = 920\ eV, \hbar\omega, 15°)$ (dotted line) and $K_{sc}^{R\ EELS}(E = 920\ eV, \hbar\omega, 15°, 15°)$ spectra for Cu.

as (for a given angle of emission θ that is not written explicitly in the equation):

$$J(E) \propto F(E) + \lambda_{sc} \int_E^{\infty} F(E') K_{sc}^{AES}(E_0, E' - E) dE' + \sum_{n=2}^{\infty} J_n \quad (3)$$

where $F(E)$ is the primary excited spectrum, $K_{sc}^{AES}(E_0, E' - E)$ the inelastic scattering cross-section as defined above for an energy loss $E' - E$ evaluated for electrons with kinetic energy E_0 and λ_{sc} the inelastic scattering mean free path defined as

$$\lambda_{sc}(E, \theta) = \left[\int_0^{\infty} K_{sc}^{AES}(E, \hbar\omega, \theta) d\hbar\omega \right]^{-1}. \quad (4)$$

The last term in Eq. (3) describes the contribution from multiple scattered electrons to the spectrum: $J_2(E)$ is the double scattering contribution, $J_3(E)$ the triple scattering contribution, and so on. The full spectrum $J(E)$ is thus modeled by repeated convolution, accounting for multiple losses.

The function $F(E)$, which is an input in the calculations, takes into account all effects related to the initial Auger process (L–S coupling and vacancy satellite effects). The shape of each peak is modeled by a symmetric mixed Gaussian–Lorentzian function [25]:

$$f_i(E) = \frac{exp\left[-4(ln2) M_i (E - E_{0i})^2 / \beta_i^2\right]}{1 + 4(1 - M_i)(E - E_{0i})^2 / \beta_i^2} \quad (5)$$

where E_{0i} is the peak center, β_i the full width at half maximum and the parameter M_i denotes the mixing ratio and takes the value of 1 for a pure Gaussian function and 0 for a pure Lorentzian function. Eq. (5) was chosen because it has been used for many years by several groups to describe a large variety of spectra and moreover it gives a certain flexibility in the fitting procedure. Thus the total primary spectrum $F(E)$ is the sum of contributions from peaks

$$F_i(E) = \frac{f_i(E)}{\int f_i(E) dE} A_{0i} \quad (6)$$

where A_{0i} is the peak area. To determine the number of peaks contributing to $F(E)$ in the fitting procedure, we were guided by the expected number of transitions predicted from previous theoretical studies [3,4]. Then the intensity of the resulting peaks $F_i(E)$ will be compared to these theoretical calculations.

Two limitations of the model have to be mentioned. First, we have assumed that the same inelastic scattering cross section K_{sc}^{AES} can be used to account not only for the first inelastic scattering but also for the multiple inelastic scattered electrons. This approximation implies an overestimation of the core-hole effect because the multiple scattered electrons are expected to be essentially unaffected by the electron–hole interaction. However, we have shown in Ref. [11] that, in the case of XPS simulations, this overestimation is weak and does not significantly influence the results. In this study we show that the same conclusion is valid for Auger calculations (see Section 1).

Second, elastic scattering processes are ignored in the model. This is justified because it was shown in Ref. [12] that the effect of elastic electron scattering is only significant for large energy losses (> ~ 30 eV).

3. Experimental setup

The experiments were performed in an UHV chamber with an Al Kα X-ray source and a VG Instruments hemispherical electron energy analyzer (VG-CLAM). The base pressure was in the 10^{-11} Torr range. The analyzer was operated in the constant pass energy mode and measured intensity distributions were corrected for the analyzer transmission function which in this mode is proportional to $E^{-0.7}$ where E is the electron kinetic energy.

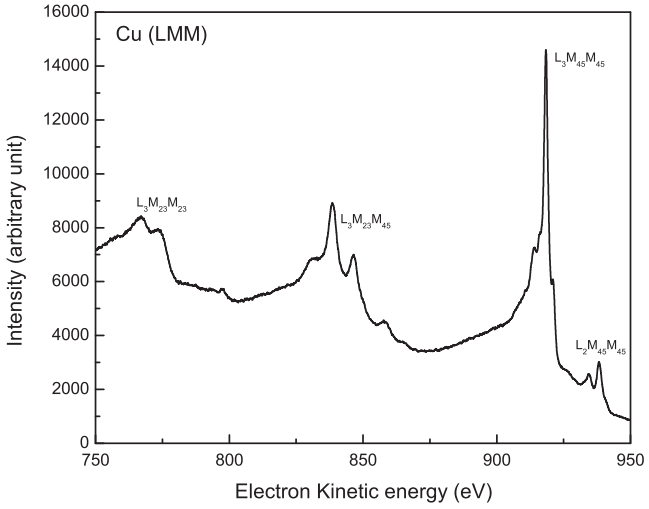

Fig. 2. Experimental Al Kα XAES spectrum of Cu. The four studied LMM Auger transitions are pointed out.

The polycrystalline high-purity Copper sample was introduced in the UHV chamber and sputtered by Ar^+ ions in order to remove any oxides or impurities present on the surface. After the Ar^+ etching, the Cu surface is expected to be largely amorphous and its contamination was found to be below the 1% level. Possible crystallinity effects are therefore expected to be negligible. The full measured XAES Cu spectrum is presented in Fig. 2.

4. Results and discussion

In this work we have studied the $L_3M_{45}M_{45}$, $L_3M_{23}M_{45}$, $L_3M_{23}M_{23}$ and $L_2M_{45}M_{45}$ Auger transitions from Cu obtained from XAES with the procedure explained in Section 2 and obtain the corresponding $F(E)$ primary excited spectra. For each transition, we compare our result with theoretical calculations of the Auger transitions [3,4].

4.1. $L_3M_{45}M_{45}$

This main Cu Auger transition arises from a single L_3 ($2p_{3/2}$) core-hole decay via the Auger process involving two M_{45} ($3d$) electrons resulting in a final $3d^8$ configuration. We then expect to observe a final state term splitting from L–S coupling, namely ^{3}F, ^{1}D, ^{3}P, ^{1}G and ^{1}S corresponding to two d holes. We will refer to this contribution as the "normal" Auger contribution to the measured $L_3M_{45}M_{45}$ transition. The energy position of the final state terms have been measured and the corresponding transition probabilities have been calculated in Ref. [3] for instance. Moreover, for Cu there is an extra structure in the low energy part of the $L_3M_{45}M_{45}$ spectrum [4,26,27] which can be explained by the occurrence of a $L_2L_3M_{45}$ Coster–Kronig transition. Indeed, after a $L_2L_3M_{45}$ Coster–Kronig transition, a $L_3M_{45}M_{45}$ process can occur with an extra hole in the M_{45} level of the initial state. The common $L_3M_{45}M_{45}$ process is thus shifted to lower kinetic energy because of the Coulomb interaction between this M_{45} spectator vacancy and the Auger electron. Moreover, the multiplet structure associated with such an Auger vacancy satellite transition corresponds to a $3d^7$ configuration. We will refer to this contribution as the "extra" Auger contribution to the measured $L_3M_{45}M_{45}$ transition. In Ref. [4], Antonides et al. have calculated that this Auger vacancy satellite structure is characterized by an energy shift of about 5 eV and an intensity of about 30% relative to the common $L_3M_{45}M_{45}$ structure, but the inaccuracy of their background subtraction procedure prevented them from making a quantitative comparison with experiment. In fact, they have only considered the two most

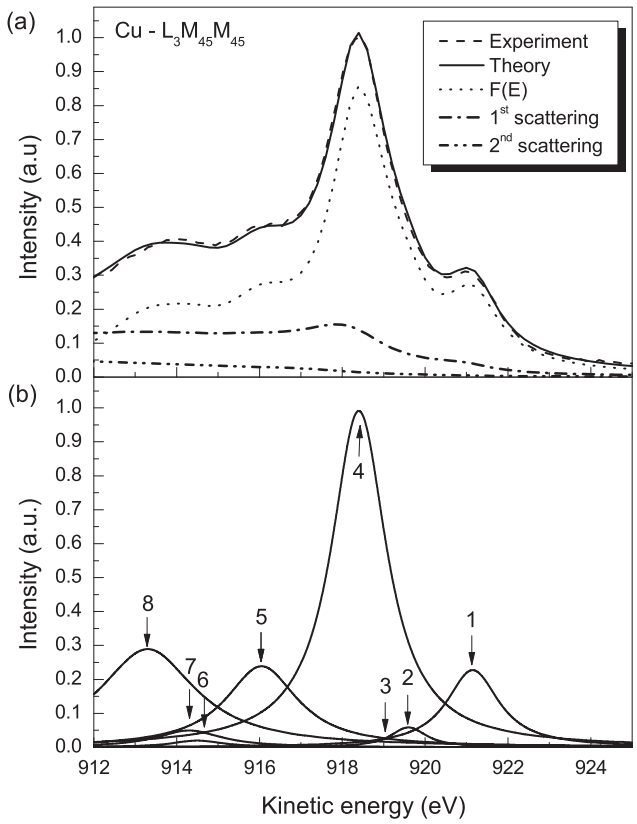

Fig. 3. Cu $L_3M_{45}M_{45}$ from pure Cu: (a) total theoretical spectrum (solid line), experimental spectrum (dashed line), $F(E)$ primary spectrum (dotted line), first (dash–dot) and second (dash–dot–dot) individual scattering contributions; and (b) various peaks contributing to the total $F(E)$ function (peaks are referenced as it is done in Table 1).

prominent peaks of this extra structure in their work, but in the present paper we find that three extra peaks are necessary to reproduce the full $L_3M_{45}M_{45}$ Auger transition observed experimentally. In accordance with these comments, we have used 8 peaks to fit the Cu $L_3M_{45}M_{45}$ transition.

Fig. 3 shows the result of this fitting procedure. Fig. 3(a) shows the determined $F(E)$ primary spectrum, the contribution from single and double inelastic scattering which are the most significant contributions as well as the sum of $F(E)$ plus multiple scattering contributions up to the eighth order denoted "Theory". The 1st and 2nd scattering contributions are not shown in the following figures. Fig. 3(b) shows separately various peaks of the transition. Each peak is labeled in accordance with Table 1 and the parameters used in $F(E)$ (E_0, A_0, β and M) are listed in Table 1. Δ is the energy difference with respect to the largest peak (i.e. ^{1}G). We also display the final state term; the * denotes the Auger vacancy satellite structure and the label "sum" denotes the combination of 5 final state terms (^{4}P, ^{2}G, ^{2}P, ^{2}H and ^{2}D) that cannot be separated. Finally, the theoretical intensities (A_t) for each individual term calculated from perturbation theory [3,4] are also shown.

Table 1
Parameters (E_0, A_0, β and M) used in $F(E)$ for Cu $L_3M_{45}M_{45}$ emission as defined by Eqs. (5) and (6). Δ gives the energy difference with respect to the largest peak (^{1}G). The final state term is also displayed (the * denotes the Auger vacancy satellite structure) as well as the theoretical intensity calculated in Ref. [3].

Peak	Term	E_0 (eV)	Δ (eV)	A_0	β (eV)	M	A_t
1	^{3}F	921.15	−2.75	0.23	1.5	0.0	0.39
2	^{1}D	919.60	−1.20	0.06	1.0	0.0	0.17
3	^{3}P	919.10	−0.70	0.04	1.0	0.0	0.03
4	^{1}G	918.40	0.00	1.00	1.6	0.0	1.00
5	^{4}F*	916.05	2.35	0.24	2.1	0.0	0.13
6	Sum*	914.50	3.90	0.02	1.5	0.0	0.06
7	^{1}S	914.30	4.10	0.05	1.9	0.0	0.03
8	^{2}F*	913.30	5.10	0.29	2.8	0.0	0.33

From these results, we can conclude that we obtain a quite good agreement between our A_0 determined from the fitting procedure and the theoretical A_t. There is a constant energy difference, namely 5.1 eV, between the "normal" Auger structure (peaks 1, 2 and 4) and the "extra" structure (peaks 5, 6 and 8) due to the vacancy as obtained in Ref. [4]. We find that (see Table 1) the ratio of the total intensity contribution from the "extra" structure to the total intensity contribution of the "normal" structure is 40% which should be compared to 30% estimated in Ref. [4]. Concerning the intensities of the individual terms, the mean difference between A_0 and A_t is about 35% which is still considered to be reasonable.

Moreover, we observe that the 2nd scattering contribution to the total spectrum shown in Fig. 3(a) is small and smooth for the energy range considered here. The use of the same inelastic scattering cross section for single and multiple losses has thus no significant influence on the results, as was also previously shown to be the case for XPS calculations [11].

4.2. $L_3M_{23}M_{45}$

The $L_3M_{23}M_{45}$ transitions are the second most intense feature among the LMM transitions for Cu. The possible final states for the main structure are ^{3}F, ^{1}D, ^{3}P, ^{3}D, ^{1}P and ^{1}F [3] but again an extra structure is present due to a M_{45} spectator vacancy following a $L_2L_3M_{45}$ Coster–Kronig transition. In Ref. [28], the relative kinetic energy of this extra structure was estimated to be shifted by about 8 eV. Fig. 4 shows the result of the fitting procedure and the parameters of the $F(E)$ function are displayed in Table 2. To our knowledge, the final states of the Auger vacancy

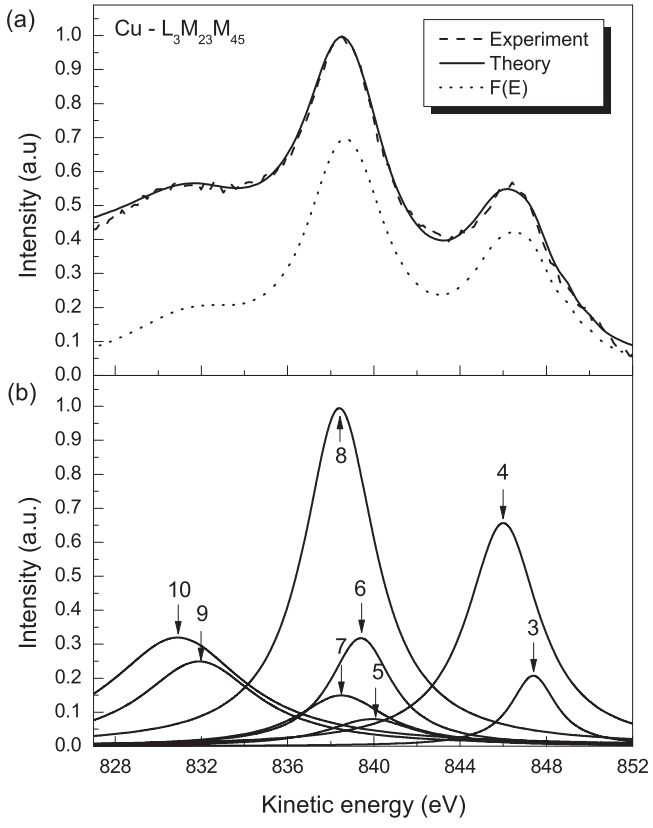

Fig. 4. Cu $L_3M_{23}M_{45}$ from pure Cu: (a) total simulated spectrum (solid line), experimental spectrum (dashed line) and $F(E)$ primary spectrum (dotted line); and (b) various peaks contributing to the total $F(E)$ function (peaks 1 and 2 are not shown because of their too small intensities).

Table 2
Parameters (E_0, A_0, β and M) used in $F(E)$ for Cu $L_3M_{23}M_{45}$ emission as defined by Eqs. (5) and (6). Δ gives the energy difference with respect to the largest peak (^{1}F). The final state term is also displayed (the * denotes the Auger vacancy satellite structure) as well as the theoretical intensity calculated in Ref. [3].

Peak	Term	E_0 (eV)	Δ (eV)	A_0	β (eV)	M	A_t
1	^{3}F	850.0	−11.6	0.01	1.0	0.0	0.01
2	^{1}D	849.0	−10.6	0.02	1.0	0.0	0.02
3	^{3}P	847.4	−9.0	0.21	2.5	0.0	0.21
4	^{3}D	846.0	−7.6	0.66	4.0	0.0	0.59
5	*	839.9	−1.5	0.08	5.0	0.0	–
6	^{1}P	839.4	−1.0	0.32	3.5	0.0	0.28
7	*	838.5	−0.1	0.15	5.0	0.0	–
8	^{1}F	838.4	0.0	1.00	4.0	0.0	1.00
9	*	831.9	6.5	0.25	6.5	0.0	–
10	*	830.9	7.5	0.32	7.5	0.0	–

satellite structure have never been published before and are only pointed out by an asterisk in the Table.

Theoretical data and results obtained from our procedure agree very well. For the "extra" structure, we have considered four peaks (peaks 5, 7, 9 and 10) that are shifted by an energy of 7.5 eV in comparison to the four more intense peaks of the "normal" structure (peaks 3, 4, 6 and 8). The previous estimated shift of about 8 eV obtained in Ref. [28] is in good agreement with this result. To reproduce the experiment we find that the intensity of the "extra" contribution to $L_3M_{23}M_{45}$ is 36% of the intensity of the "normal" emission. This is similar to the 40% relative intensity found for the $L_3M_{45}M_{45}$ transition (see the previous section). Note that the mean difference between the intensities of the individual terms A_0 and A_t is only ~ 5% (except for peak 9 for which the difference is much larger).

Table 3
Parameters (E_0, A_0, β and M) used in $F(E)$ for Cu $L_3M_{23}M_{23}$ emission as defined by Eqs. (5) and (6). Δ gives the energy difference with respect to the largest peak (^{3}P). The final state term is also displayed as well as the theoretical intensity calculated in Ref. [3].

Peak	Term	E_0 (eV)	Δ (eV)	A_0	β (eV)	M	A_t
1	^{3}P	773.9	0.0	1.00	6.0	1.0	1.00
2	^{1}D	767.2	6.7	0.96	6.0	1.0	0.85
3	^{1}S	762.0	11.9	0.27	6.0	1.0	0.24
4	??	759.1	15.8	0.45	9.0	1.0	–

4.3. $L_3M_{23}M_{23}$

Results for the $L_3M_{23}M_{23}$ structure are shown in Fig. 5 and Table 3. Due to the larger binding energy of the M_{23} state (in comparison to the M_{45} state), there is no influence from the previously mentioned Coster–Kronig transition and thus the Auger spectrum for the $L_3M_{23}M_{23}$ is clearer. Indeed, the three possible final states (^{3}P, ^{1}D, ^{1}S) are present with intensities in reasonable agreement with theory [3] (~ 12% mean deviation between the individual A_0 and A_t). However, we observe the presence of an undetermined peak (peak 4 in Table 3). This peak is also present in experimental works that can be found in the literature [2,3,29] but no explanation has been proposed for its origin. We emphasize here that the main advantage of our analysis method is that it allows to determine accurate peak positions and intensities from experimental spectra and that this can thus help for a better understanding of the mechanisms of the transitions. For the other peaks, the agreement between our results and theoretical results from Ref. [3] is quite good.

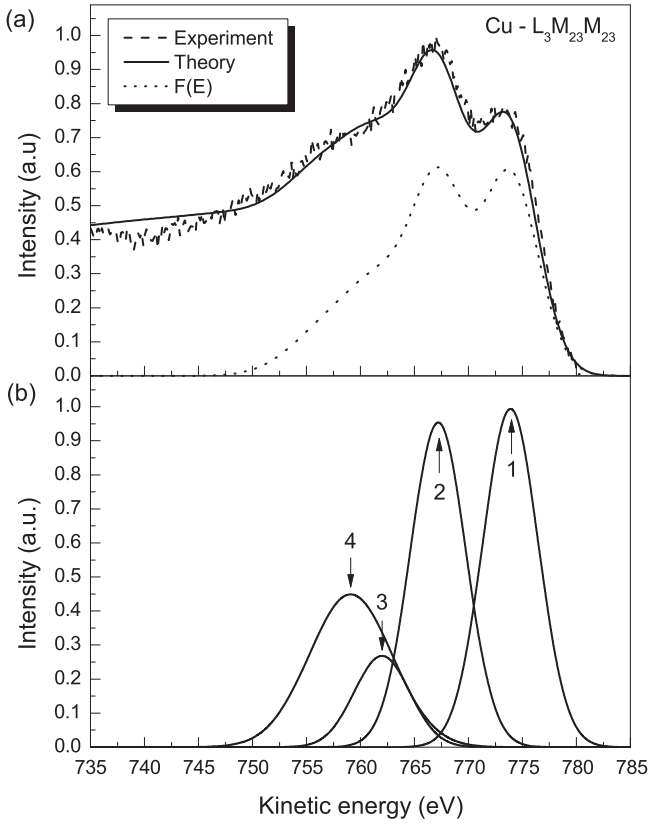

Fig. 5. Cu $L_3M_{23}M_{23}$ from pure Cu: (a) total simulated spectrum (solid line), experimental spectrum (dashed line) and $F(E)$ primary spectrum (dotted line); and (b) various peaks contributing to the total $F(E)$ function.

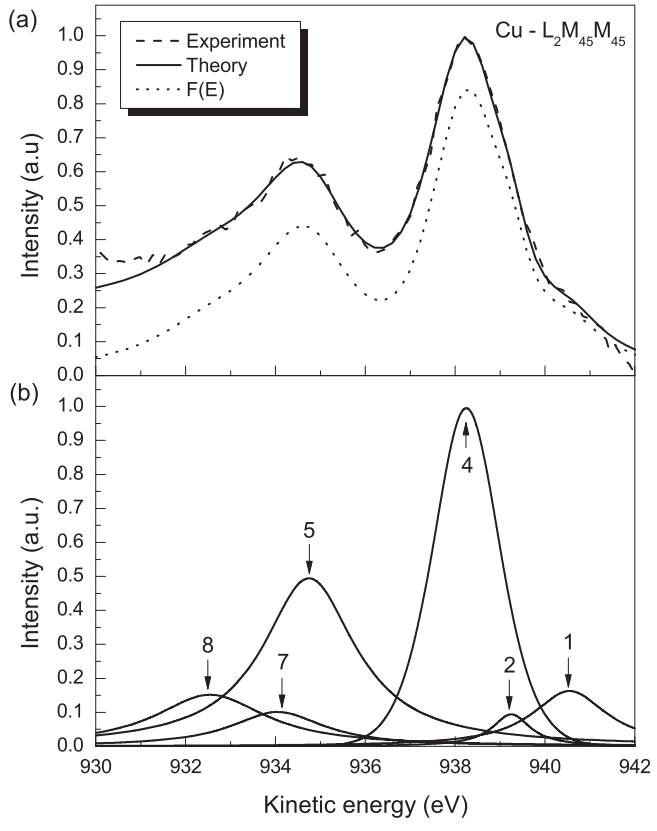

Fig. 6. Cu $L_2M_{45}M_{45}$ from pure Cu: (a) total simulated spectrum (solid line), experimental spectrum (dashed line) and $F(E)$ primary spectrum (dotted line); and (b) various peaks contributing to the total $F(E)$ function (peaks 3 and 6 are not shown because of their too small intensities).

Table 4
Parameters (E_0, A_0, β and M) used in $F(E)$ for Cu $L_2M_{45}M_{45}$ emission as defined by Eqs. (5) and (6). Δ gives the energy difference with respect to the largest peak (^{3}P). The final state term is also displayed as well as the theoretical intensity calculated in Ref. [3].

Peak	Term	E_0 (eV)	Δ (eV)	A_0	β (eV)	M	A_t
1	^{3}F	940.55	−2.3	0.29	2.0	0.0	0.38
2	^{1}D	939.25	−1.0	0.17	1.0	0.0	0.17
3	^{3}P	938.65	−0.4	0.02	1.5	0.0	0.03
4	^{1}G	938.25	0.0	1.00	1.8	0.5	1.00
5	??	934.75	3.5	0.88	2.5	0.0	–
6	^{1}S	934.35	3.9	0.01	1.5	0.0	0.02
7	??	934.05	4.2	0.18	2.5	0.0	–
8	??	932.55	5.7	0.27	3.0	0.0	–

4.4. $L_2M_{45}M_{45}$

Fig. 6 and Table 4 show results obtained for the $L_2M_{45}M_{45}$ transition. From a theoretical point of view, some ambiguities exist for the $L_2M_{45}M_{45}$ transition and a definite interpretation has not been found yet. Indeed, beside the "normal structure" (^{3}F, ^{1}D, ^{3}P, ^{1}G and ^{1}S) [3], the Auger spectrum shows a "satellite" structure (peaks 5, 7, 8) which accounts for 50% of the total intensity. Various explanations have been proposed for this structure. It has been suggested [26] that it is due to a $L_1L_2M_{45}$ Coster–Kronig transition preceding the $L_2M_{45}M_{45}$ involving thus a M_{45} spectator vacancy but this interpretation is questioned by Sarma et al. [30] who argue that the satellites are produced by final-state shake-off while Thurgate and Neale [31] propose an initial-state shake-up to explain the $L_2M_{45}M_{45}$ behavior. Finally, in Ref. [5], the satellite structure was explained by a combination of Coster–Kronig, shake-off and shake-up processes.

It is clearly not the goal of this paper to propose an interpretation of the $L_2M_{45}M_{45}$ feature but again the present more precise analysis of the experiment can hopefully lead to a clarification of this problem. Finally, for the "normal structure", our experimentally determined intensities agree with theoretical results of Antonides et al. [3] with less than 10% mean difference between A_0 and A_t (see Table 4).

5. Conclusion

We have quantitatively determined the relative contributions from various Auger processes for copper, more specifically the $L_3M_{45}M_{45}$, $L_3M_{23}M_{45}$, $L_3M_{23}M_{23}$ and $L_2M_{45}M_{45}$ Auger transitions, and determined the corresponding primary excitation spectra. This was done by first calculating the effective differential inelastic scattering cross section for XAES within the semi-classical dielectric response model which includes the effects of the two core holes and of the surface as well as interference effects. This cross section was then convoluted with a model primary spectrum which was varied until good agreement with the experimental XAES was obtained. Within the limitations of the model, it allows to accurately determine the primary excitation spectrum for Auger transitions where the effects of both extrinsic and intrinsic energy loss contributions as well as the effect of surface excitations have been removed.

We compare the determined primary excitation Auger spectra with previously published theoretical results and obtain a reasonable agreement. This procedure thus allows to extract quantitative information from XAES experiments which can be compared with potential theoretical calculations and finally lead to a better understanding of the mechanisms behind Auger transitions.

Thus, we have shown that with our procedure it is possible from experimental spectra to extract quantitative information on the Coster–Kronig, shake-off and shake-up processes that compete with the "normal" Auger process.

Acknowledgments

F.Y. and S.T. thank the Spanish Ministry of Economy and Competitiveness (Projects CONSOLIDER-CSD 2008-00023, MAT2013-40852-R) and the Danish Council for Independent Research (Natural Sciences) for financial support.

References

[1] D. Briggs, J.T. Grant (Eds.), Surface Analysis by Auger and X-ray Photoelectron Spectroscopy, IM-Publications, Chichester, 2003.
[2] E.J. McGuire, Phys. Rev. A 16 (1977) 2365.
[3] E. Antonides, E.C. Janse, G.A. Sawatzky, Phys. Rev. B 15 (1977) 1669.
[4] E. Antonides, E.C. Janse, G.A. Sawatzky, Phys. Rev. B 15 (1977) 4596.
[5] D.D. Sarma, S.R. Barman, R. Cimino, C. Carbone, P. Sen, A. Roy, A. Chainani, W. Gudat, Phys. Rev. B 48 (1993) 6822.
[6] A. Tanaka, T. Nakamura, K. Hirokawa, Appl. Surf. Sci. 169–170 (2001) 160.
[7] M. Ohno, J. Electron. Spectrosc. Relat. Phenom. 164 (2008) 1.
[8] D.A. Shirley, Phys. Rev. B 5 (1972) 4709.
[9] J. Vegh, Surf. Sci. 577 (2005) 220.
[10] S. Tougaard, Surf. Sci. 216 (1989) 343.
[11] N. Pauly, S. Tougaard, F. Yubero, Surf. Sci. 620 (2014) 17.
[12] N. Pauly, S. Tougaard, F. Yubero, Surf. Interface Anal. (2014), http://dx.doi.org/10.1002/sia.5372.
[13] S. Tougaard, F. Yubero, Surf. Interface Anal. 36 (2004) 824 (The software is available free of charge at www.quases.com).
[14] S. Tougaard, F. Yubero, Surf. Interface Anal. 44 (2012) 1114.
[15] A.C. Simonsen, F. Yubero, S. Tougaard, Phys. Rev. B 56 (1997) 1612.
[16] F. Yubero, S.S. Tougaard, Phys. Rev. B 71 (2005) 045414.
[17] J.L. Gervasoni, N.R. Arista, Surf. Sci. 260 (1992) 329.
[18] F. Yubero, L. Kövér, W. Drube, Th. Eickhoff, S. Tougaard, Surf. Sci. 592 (2005) 1.
[19] F. Yubero, S. Tougaard, J. Electron Spectrosc. Relat. Phenom. 185 (2012) 552.
[20] Z. Berényi, L. Kövér, S. Tougaard, F. Yubero, J. Tóth, I. Cserny, D. Varga, J. Electron Spectrosc. Relat. Phenom. 135 (2004) 177.
[21] F. Yubero, J.M. Sanz, B. Ramskov, S. Tougaard, Phys. Rev. B 53 (1996) 9719.
[22] R.H. Ritchie, A. Howie, Philos. Mag. 36 (1977) 463.
[23] D. Tahir, S.S. Tougaard, J. Phys. Condens. Matter 24 (2012) 175002.
[24] S. Tougaard, P. Sigmund, Phys. Rev. B 25 (1982) 4452.
[25] D. Briggs, M.P. Seah (Eds.), Practical Surface Analysis, vol. 1, Wiley, Chichester, 1990.
[26] E.D. Roberts, P. Weightman, C.E. Johnson, J. Phys. C Solid State Phys. 8 (1975) L301.
[27] J.C. Fuggle, P. Bennett, F.U. Hillebrecht, A. Lenselink, G.A. Sawatzky, Phys. Rev. Lett. 49 (1982) 1787.
[28] G. van der Laan, C. Westra, C. Haas, G.A. Sawatzky, Phys. Rev. B 23 (1981) 4369.
[29] J.F. Mc Gilp, P. Weightman, J. Phys. C Solid State Phys. 11 (1978) 643.
[30] D.D. Sarma, C. Carbone, P. Sen, R. Cimino, W. Gudat, Phys. Rev. Lett. 63 (1989) 656.
[31] S.M. Thurgate, J. Neale, Surf. Sci. Lett. 256 (1991) L605.